

## SUMMARY OF FLUIDIC THRUST VECTORING RESEARCH CONDUCTED AT NASA Langley Research Center

Karen A. Deere<sup>\*</sup>  
NASA Langley Research Center  
Hampton, VA 23681

### ABSTRACT

Interest in low-observable aircraft and in lowering an aircraft's exhaust system weight sparked decades of research for fixed geometry exhaust nozzles. The desire for such integrated exhaust nozzles was the catalyst for new fluidic control techniques; including throat area control, expansion control, and thrust-vector angle control. This paper summarizes a variety of fluidic thrust vectoring concepts that have been tested both experimentally and computationally at NASA Langley Research Center. The nozzle concepts are divided into three categories according to the method used for fluidic thrust vectoring: the shock vector control method, the throat shifting method, and the counterflow method. This paper explains the thrust vectoring mechanism for each fluidic method, provides examples of configurations tested for each method, and discusses the advantages and disadvantages of each method.

### INTRODUCTION

Maintaining United States air supremacy requires an elite Air Force with stealthy, supermaneuverable aircraft. Decades of research on mechanical thrust vectoring techniques was initiated in the 1970's to meet the demand for fighter aircraft with increased agility. Additional requirements for low-observable aircraft and for lower exhaust system weights were the catalysts for research on fluidic control of nozzles in the 1990's. The research completed by NASA Langley Research Center (LaRC) in collaboration with the United States Air Force (USAF), industry, and academia partners now comprises an extraordinary database of fluidic control techniques that empowers researchers with

the freedom to explore conceptual designs for lightweight, low-observable exhaust nozzles.

Many of the collaborative programs conducted at NASA LaRC were focused on fixed-aperture nozzle concepts. Researchers embarked on fluidic control techniques, with visions of integrated exhaust nozzles, containing no moving parts. The potential benefits of fluidic thrust vectoring nozzles, over fully-mechanical schemes, were estimated in the NASA and USAF Fluidic Injection Nozzle Technology (FLINT) program (ref. 1) as a 28-40% weight reduction by implementing fluidic throat area control, a 43-80% weight reduction by implementing fluidic throat area and exit area control, a 7-12% improvement in engine thrust-to-weight ratio, and a 37-53% reduction in nozzle procurement and life cycle costs. In addition, fixed aperture nozzles would enhance low-observable integration aspects by eliminating moving flaps, discontinuities, and gaps.

This paper is intended to provide a summary of the fluidic thrust vectoring concepts investigated both experimentally and computationally at NASA LaRC. Since the exhaust flows associated with fluidic thrust vectoring concepts are highly complex, only a brief summary of the investigations are provided herein. The reader is encouraged to examine the details of the complexity of the fluidic thrust vectoring concepts in the designated references. The nozzle concepts are divided into the three categories according to the method used for fluidic thrust vectoring: the shock vector control method, the throat shifting method, and the counterflow method. The discussion section will explain the thrust vectoring mechanism for each fluidic method, provide examples of configurations tested for each method, and discuss the advantages and disadvantages of each method.

\* Aerospace Engineer, Configuration Aerodynamics Branch, AIAA Senior Member

This material is declared a work of the U.S. Government and is not subject to copyright protection in the United States.

## NOMENCLATURE

### Symbols:

$A_e$	exit area, in <sup>2</sup>
$A_t$	minimum ("throat") area, in <sup>2</sup>
$C_{fg,sys}$	system thrust ratio, $F_r / (F_{i,p} + F_{i,s})$
$F_r$	resultant thrust
$F_{i,p}$	ideal isentropic thrust of primary flow
$F_{i,s}$	ideal isentropic thrust of injection flow
$H$	Counterflow Nozzle primary jet height, in
$L$	Counterflow Nozzle suction collar length, in
$p_{amb}$	ambient pressure, psi
$p_{slot}$	static pressure at suction slot exit, psi
$p_{t,e}$	ejector total pressure, psi
$p_{t,j}$	primary jet total pressure, psi
$p_{t,s}$	secondary total pressure, psi
$p_2$	upper secondary slot static pressure, psi
$p_3$	lower secondary slot static pressure, psi
$\Delta p_{slot}$	average differential (suction) static pressure at primary nozzle exit (slot), $p_{amb} - p_{slot}$ , psi
$U_1$	primary nozzle exit velocity, ft/s
$x$	distance downstream of upstream minimum, in.
$z$	distance above nozzle centerline, in.
$\delta_p$	pitch thrust-vector angle, deg
$\delta_y$	yaw thrust-vector angle, deg
$\epsilon$	expansion ratio, $A_e/A_t$
$\rho_1$	primary nozzle exit density, slug/ft <sup>3</sup>
$\phi$	fluidic injection angle, deg
$\eta$	thrust-vectoring efficiency, deg/percent injection
$\lambda$	suction parameter, $(p_3 - p_2)L / (\rho_1 U_1^2)^*H$

### Abbreviations:

AXI	axisymmetric
2D	two-dimensional
CD	convergent-divergent
EPR	ejector pressure ratio, $p_{t,e} / p_{t,j}$
FYVN	Fluidic Yaw Vector Nozzle
JETF	Jet Exit Test Facility
LOLA	Low Observable, Lightweight, Affordable
MATV	multi-axis thrust vectoring
NPR	nozzle pressure ratio, $p_{i,j} / p_{amb}$
NPR <sub>D</sub>	design nozzle pressure ratio
PTV	pitch thrust vectoring
SALIENT	Survivable Affordable Lightweight Integrated Exhaust Nozzle Technologies
SPR	secondary pressure ratio, $p_{t,s} / p_{t,j}$
SVC	shock vector control
TS	throat shifting

## FLUIDIC THRUST VECTORING CONCEPTS

Fluidic control in exhaust nozzles includes throat area, expansion ratio, and thrust-vector angle. While the former two are equally important, the resources at

NASA LaRC were focused on investigating fluidic thrust vectoring techniques. Promising concepts were investigated with computational and experimental tools, as well as system studies when appropriate. The cooperative teams collaborated on the design and testing of the hardware, with Langley researchers typically leading experimental testing in the NASA LaRC Jet Exit Test Facility (JETF) and the industry partners generally leading the design of the nozzle. It is important to note that fluidic research has been conducted independent of NASA and this paper will only discuss work conducted at NASA LaRC.

Fluidic thrust vectoring methods tend to fall into three basic categories: shock vector control (SVC), throat shifting (TS), and counterflow methods. The eight nozzle concepts listed in Table 1 were used to investigate the shock vector control method of fluidic thrust vectoring (refs. 2-10). The nozzle concepts utilized to investigate the throat shifting method of fluidic thrust vectoring are listed in Table 2 (refs. 11-12). The nozzle concept listed in Table 3 was used to investigate a combination of the shock vector control and the throat shifting methods for multi-axis thrust vectoring (MATV) in a fixed aperture nozzle. Research completed on the counterflow thrust vectoring method is listed in Table 4 (refs. 13-14).

## EXPERIMENTAL FACILITY DESCRIPTION

### Jet Exit Test Facility

All of the experimental fluidic thrust vectoring work conducted at NASA LaRC that is summarized herein, was completed in the Jet Exit Test Facility (JETF). Internal nozzle performance is obtained in JETF by simulating propulsion flows at static (wind-off) conditions. The test apparatus consists of a propulsion simulation system, two independently controllable air supply systems, and a data acquisition room. The primary and secondary air-supply systems are each capable of delivering air at approximately 23 lb/sec to the test stand. The high-pressure air supply system provides clean, dry air at a constant total temperature near 530 R. Test articles are mounted on the propulsion simulation system in a soundproof room with an air exhaust collector duct downstream of the exhaust jet. A complete description of JETF can be found in reference 15.

### Propulsion Simulation System

The single-engine propulsion simulation system, shown in figure 1, was used for one test discussed in this paper. The rest of the experimental tests were conducted on the dual-flow propulsion simulation system (ref. 15). The dual-flow system mounted on

the static thrust stand is shown in figure 2(a) and a detailed sketch of the hardware is shown in figure 2(b). This system contains two isolated co-annular flow paths for primary and secondary flows, with each of the flow paths containing a plenum and an instrumentation section. The co-annular arrangement was designed for testing dual-flow, axisymmetric turbofan exhaust nozzles. However, for fluidic thrust vectoring tests, the secondary annular flow can be capped off, allowing attachment of secondary air lines and control valves for fluidic injection.

Independently controlled primary and secondary flow systems provide pressurized air to isolated plenum chambers on the propulsion system through two pairs of semirigid, thin-walled (0.021-in. wall thickness), 1-in. diameter, S-shaped, stainless steel tubes (S-tubes). The S-tubes, shown in figure 2(a), were designed to minimize balance tares caused by flexure during increased pressurization or by the transfer of axial momentum as air is transferred from the nonmetric to the metric part (supported by the force balance) of the system. This design provides repeatable force and moment tares. System calibrations are completed so that the final data reflects only forces and moments produced by the test article. The primary and secondary air systems can be used separately or in combination for dual-flow operation. The two independent flow streams each pass through a multiple critical venturi system (ref. 16) where the flow rate of each air stream is measured to within a 0.1 percent measurement uncertainty.

The air supplied to the propulsion system is discharged in a radial fashion through eight equally spaced sonic nozzles, from the primary plenum into an annular low-pressure duct (on the model centerline). The airflow then passes over an aerodynamic balance fairing and through an axisymmetric choke plate that provides a pressure drop to encourage a uniform flow field. Downstream of the choke plate, the air passes through the axisymmetric primary instrumentation section and then through the test article. The airflow exhausts to atmospheric conditions in a test bay with louvered ceiling vents to channel the flow outside the facility.

### COMPUTATIONAL DESCRIPTION

The computational fluid dynamics (CFD) code PAB3D was developed for and has been used to accurately predict propulsive flows with mixing, separated flow regions, and jet shear layers (refs. 17-19). PAB3D solves the three-dimensional, Reynolds-averaged Navier-Stokes (RANS) equations and uses one of several turbulence models for closure of the

RANS equations. The governing equations are written in generalized coordinates and in conservative form. In an effort to decrease computational resources, the simplified, thin-layer Navier-Stokes equations are implemented into PAB3D. This approximation neglects derivatives in the viscous terms streamwise and parallel to the surface, since they are typically negligible in comparison to the derivatives normal to the surface.

The PAB3D flow solver was written with three numerical schemes: the flux vector-splitting scheme of van Leer (ref. 20), the flux difference-splitting scheme of Roe (ref. 21), and a modified Roe scheme primarily used for space marching solutions. These schemes implement the finite volume principle to balance the fluxes across grid cells and the upwind biased scheme of van Leer or Roe to determine fluxes at the cell interfaces. Only the inviscid terms of the flux vectors are split and upwind differenced, while the diffusion terms of the Navier-Stokes equations are central differenced.

Turbulence simulations are computed within PAB3D by implementing an algebraic, a linear 2-equation, or a nonlinear 2-equation turbulence model. The 2-equation turbulence model, with second order closure, is used to model more complex viscous flow features. The pair of coupled transport equations; turbulent kinetic energy and turbulent energy dissipation rate, are written in conservative form and can be uncoupled from the Navier-Stokes equations and from each other to decrease computational requirements. Extensive details of PAB3D are found in references 17-23.

In an effort to simulate a configuration tested at static (wind-off) freestream conditions, a small freestream Mach number ( $M=0.05$ ) is generally implemented to reduce error and aid the stability of the computational solution.

### DISCUSSION

Mechanical thrust vectoring nozzles use actuated hardware to manipulate the primary exhaust flow. Although mechanical thrust vectoring schemes are highly effective, the actuator hardware can create a heavy, complex propulsion system that, with gaps and discontinuities, is an obvious target for radar detection. In an effort to develop less detectable, light-weight, fixed geometry nozzles with low parts count, research was shifted from mechanical thrust vectoring schemes to fluidic thrust vectoring methods in the 1990's. Fluidic thrust vectoring nozzles use a secondary air source to create an off-axis deflection of the primary jet thrust vector. Three primary methods of fluidic thrust vectoring have been

investigated over the past decade; the shock vector control (SVC) method, the throat shifting (TS) method, and the counterflow method. Each method uses the secondary air source in a different way, as discussed in separate sections below. However, the thrust vectoring mechanism in all three methods is simply the creation of an asymmetric pressure distribution on the nozzle surfaces.

In addition to the three primary fluidic thrust vectoring methods listed above, the Coanda effect (ref. 24) was used in one concept with the shock vector control method for multiaxis thrust vectoring. The Coanda effect is the tendency of a fluid to adhere to a curved surface because of the reduced pressure caused by flow acceleration around the surface. This effect can be enhanced by injecting a thin sheet of high velocity, turbulent air tangential to the curved surface. The higher-velocity injected flow causes a low pressure region along the curved surface that attracts the larger, higher pressure main flow and causes it to follow the curved surface farther than it would without the secondary injection (delays separation). This was the technique used in reference 4 to attempt to vector the high energy jet exhaust flow in the yaw plane.

The eight nozzle concepts listed in Table 1 were used to investigate the shock vector control, fluidic thrust vectoring method. The first shock vector control concept tested at NASA LaRC in 1987 was a two-dimensional, convergent-divergent (2D CD) nozzle with fluidic pitch thrust vectoring (ref. 2). In 1992, the highly successful shock vector control method in the pitch axis was combined with a less-successful Coanda blowing method in the yaw axis for multi-axis thrust vectoring in a 2D CD nozzle concept (ref. 3-4). In 1995, a Spherical Convergent Flap Nozzle, designed with a hexagonal flow path, fluidic pitch thrust vectoring, and ejectors, was investigated with the SALIENT-I Nozzle concept. Multi-axis fluidic thrust vectoring capability was added to this concept during the testing of the SALIENT-II Nozzle in 1996 (ref. 5). The LOLA-II Nozzle and the Hybrid 2D CD Nozzle were also tested in 1996. In the LOLA-II program, fluidic pitch thrust vectoring was added to the successful fluidic throat-area control concept demonstrated with LOLA-I (ref. 6). The Hybrid 2D CD Nozzle was designed with a fixed aperture, ejectors, and a hybrid thrust vectoring scheme that included combinations of fluidic and mechanical pitch thrust vectoring (ref. 7). The axisymmetric, convergent-divergent (AXI CD) nozzle was tested in 1997 to determine the thrust vectoring and internal nozzle performance competitiveness with rectangular nonaxisymmetric nozzles (ref. 8). Since all concepts thus far had been tested at static freestream conditions, a computational

assessment of the freestream effects on fluidic thrust vectoring was initiated in 1998, using the Fluidic Jet Effects Model (ref. 9). The Multi-Slot Injection Nozzle tested at NASA LaRC in 1999, was a 2D CD nozzle designed with multiple injection slots to investigate the potential benefits of dual-slot injection over single-slot injection (ref. 10). As noted above, two of the test articles were designed with ejectors, which are used to improve off-design efficiency. Ejectors are used at over-expanded conditions to "fill" the divergent section of the nozzle with secondary air in an effort to raise static pressure and reduce overexpansion losses.

The nozzle concepts utilized to investigate the throat-shifting, fluidic thrust vectoring method are listed in Table 2. A promising twin-engine configuration and a less successful single-engine configuration, designed with a fixed aperture and lemon-shaped cross section, were investigated with the Fluidic Yaw Vectoring Nozzle (FYVN) concept in 1995. Limited computational and experimental results for FYVN are found in reference 11. The NASA LaRC developed Recessed Cavity Nozzle concept enhances the throat shifting method with separation control to achieve substantial thrust-vector angles, without detrimental impacts on thrust efficiency. PAB3D was used to guide the design of the Recessed Cavity Nozzle in a parametric computational investigation that was completed in 2002 (ref. 12). Experimental testing of this promising concept was completed in March 2003.

The test article listed in Table 3 was used to investigate the combination of the shock vector control and the throat shifting methods for MATV in a fixed aperture nozzle in 2001. Unfortunately, adding the shock vector control method for pitch thrust vectoring to the efficient yaw thrust-vectoring nozzle, optimized for the throat shifting method, was relatively unsuccessful.

The first laboratory tests of the counterflow method were conducted on a nozzle with an extremely small throat area,  $A_t=0.62 \text{ in}^2$  (ref. 25). The research completed at NASA LaRC on the counterflow thrust vectoring method is listed in Table 4. The first Langley experimental test entry in 1995 investigated thrust vectoring and nozzle performance of a larger-scale ( $A_t=3 \text{ in}^2$ ) counterflow nozzle, while the second test entry in 1998 focused on relieving hysteretic jet attachment with a porous collar (ref. 13). The first and only successful computational investigation of the counterflow method that could be found in the literature was completed with the PAB3D computational fluid dynamics code in 1999 (ref. 14).

### Shock Vector Control Method

Fluidic thrust vectoring with the shock vector control method requires forced, asymmetric fluidic injection of a secondary air stream into the supersonic, primary flow that develops in the divergent section of the nozzle at certain conditions. An oblique shock is created as the supersonic flow "sees" the secondary airflow as an obstruction. The primary exhaust flow is then diverted through the oblique shock, which can produce large thrust-vector angles, but at the expense of thrust efficiency as losses occur when the primary flow passes through the oblique shock. In addition, thrust vectoring and thrust performance penalties exist when the oblique shock, created by fluidic injection, impinges the opposing nozzle wall. The SVC method is most effective at over expanded conditions, when the oblique shock is able to eliminate the flow separation along one wall that occurs at off-design conditions. The resulting asymmetric pressure loading results in a non-zero thrust-vector angle. Unfortunately thrust performance losses are typically high at these conditions. At fully expanded conditions with no separation in the divergent section of the nozzle (typically higher thrust performance), the oblique shock is less efficient at turning the primary flow. A description of the eight investigations on shock vector control concepts will now follow.

**2D CD PTV:** The goal of this investigation was to obtain internal nozzle performance on a 2D CD nozzle with fluidic pitch thrust vectoring. A side view sketch of the 2D CD PTV Nozzle mounted on the single-engine propulsion simulation system is shown in figure 1. The geometric variables that were investigated include the axial injection location, the injection hole area, and the number of injection holes in each row. The nozzle concept had a design nozzle pressure ratio of  $NPR_D=15.6$ . The test was conducted at static freestream conditions with the nozzle operating at highly overexpanded conditions ( $NPR=2-7.5$ ). Fluidic injection conditions were set with a ratio of secondary to primary total pressure (SPR), which was varied over a range of  $SPR=0.5-7.5$ .

Results indicated that the axial injection location could significantly affect thrust-vector angle; the best injection location was near the natural shock and separation location that occurs without fluidic injection. In this study, the smallest injection holes provided the best thrust vectoring, while the injection area and number of holes and rows had minimal effects on thrust-vector angle. Thrust-vector angle increased to a maximum with increasing SPR, but then decreased as SPR continued to increase because the oblique shock strengthened and impinged on the

opposite wall. At this point, a second, weaker oblique shock reflected from the wall and caused flow turning in the opposite direction from that obtained through the first shock. As with many SVC concepts, thrust-vector angle reached a maximum at low NPR and decreased with increasing NPR. Although the best thrust-vectoring efficiency achieved with this concept was  $\eta=4.4\% \text{-injection}$ , it was at a  $NPR=3$  with poor thrust performance,  $C_{fg,sys}=0.891$ . Thrust performance improved to  $C_{fg,sys}=0.935$  by  $NPR=6$ , however, thrust-vectoring efficiency was reduced to  $\eta=2.2\% \text{-injection}$ . Even at the highest values of NPR tested, thrust performance losses resulting from overexpanded flow in the nozzle were large. A complete set of results is published in reference 2.

**2D CD MATV:** The goal of this project was to achieve multi-axis, fluidic thrust vectoring, with pitch thrust-vector angles of  $\delta_p=\pm 20^\circ$  and yaw thrust-vector angles of  $\delta_y=\pm 10^\circ$  at  $NPR=6$ . Sketches of the 2D CD MATV Nozzle concept are shown in figure 3. Figure 3(a) shows a side view sketch of the nozzle with the SVC method for pitch thrust vectoring; fluidic injection on the upper divergent wall, a shock, and the flow direction are indicated. Figure 3(b) shows a top view sketch of the nozzle with Coanda blowing on the left sidewall for yaw thrust vectoring. The geometric variables investigated include expansion ratio, pitch flap injection location, Coanda flap length and Coanda angle. The design conditions for the various expansion ratios ( $\epsilon=1.5, 1.94, \text{ and } 2.4$ ) tested were  $NPR_D=6.25, 10.2, \text{ and } 14.6$ , respectively. This concept was tested at static freestream conditions, with nozzle conditions in the range of  $NPR=2-10$  and fluidic injection flow rates up to 10% of the primary flow rate.

Results indicated that although aggressive goals were not met, practical levels of pitch thrust-vector angle were reached ( $\delta_p=14^\circ$ ) with the largest expansion ratio. Larger thrust-vector angles up to  $\delta_p=19^\circ$  were achieved with  $\epsilon=2.4$ , but only at a  $NPR=2$  with 10% injection (bleed). Therefore, the best pitch thrust-vectoring efficiency achieved with this concept was  $\eta=1.9\% \text{-injection}$  at a  $NPR=2$ , while a moderate level of  $\eta=1.4\% \text{-injection}$  was achieved at  $NPR=6$ . Thrust performance for the  $\epsilon=2.4$  configuration ranged from  $C_{fg,sys}=0.876$  at  $NPR=2$  to  $C_{fg,sys}=0.93$  at  $NPR=8$ . Decreasing expansion ratio improved thrust performance, but at the expense of thrust-vectoring efficiency.

In general, increasing injection rate improved thrust-vector angle. However, at certain conditions, the oblique shock impinged on the opposite wall and reduced thrust vectoring. A low nozzle aspect ratio

and a forward slot injection location increased the risk of shock impingement. There was an associated loss in thrust efficiency as shock strength increased with increasing NPR and SPR. Coanda blowing was unsuccessful for yaw thrust vectoring, as the flow separated from nozzle surface at  $NPR > 4$ . A complete set of results is compiled in references 3 and 4.

**Spherical Convergent Flap:** The SALIENT-I and SALIENT-II programs built on the physics uncovered in a previous mechanical thrust vectoring (non-fixed aperture) and throat area control test of the Spherical Convergent Flap Nozzle (ref. 26). The SALIENT goals were to effectively add fluidic pitch and yaw thrust vectoring capability to the Spherical Convergent Flap Nozzle and to understand the interaction between the injector, the ejector and the primary exhaust flows. The ejector was used for expansion ratio control and improved thrust efficiency. The nozzle was aggressively shaped with a fixed aperture for a low-observable design and had a hexagonal flow path with injectors on the divergent walls. A side view sketch of the Spherical Convergent Flap Nozzle is shown in figure 4(a) and a photograph of an oblique view of the model mounted in JETF is shown in figure 4(b). The geometric variables investigated include injection slot location and power setting. Expansion ratios of  $\epsilon=2.15, 1.8, 1.15$  were tested with design conditions of  $NPR_D=12, 8.7, 6.2$ , respectively. The nozzle was tested at static freestream conditions, with nozzle conditions in the range of  $NPR=2-10$ , fluidic injection conditions up to  $SPR=1.0$ , and ejector conditions up to  $EPR=0.12$ .

Successful results included reaching thrust vector angles up to  $15^\circ$  in separate pitch or yaw thrust vectoring, and up to  $10^\circ$  of multi-axis thrust vectoring. Thrust vectoring efficiencies ranged from  $1.1\%/\text{-injection}$  to  $1.4\%/\text{-injection}$  in pitch vectoring mode. Typical of SVC method, thrust efficiency was 3-4% below that of conventional variable geometry nozzles at low power. Thrust efficiency was improved with a small amount of full-perimeter ejector flow. However, increasing EPR had no improved benefit on performance. Pitch thrust vectoring with a single injection slot provided a  $1^\circ$  improvement in thrust-vector angle, with negligible differences in thrust efficiency, over that of a dual injection slot configuration. A complete set of results is compiled in reference 5.

**LOLA-II:** The goal of this project was to add MATV capability to the LOLA-I Nozzle shown in figure 5, which was previously tested and designed with fluidic throat area control for manipulating power setting. The throat area control test variables included throat injection angle and injection slot area

(ref. 6). The LOLA-II Nozzle had pitch and yaw thrust vectoring capability with an elliptical-shaped cross section at the geometric minimum area that transitioned to an iris-shaped cross section at the exit plane. The primary geometric variables investigated with LOLA-II were pitch and yaw fluidic injection angles, circumferential coverage of the throat injection slot and throat injection slot size. The nozzle was tested at static freestream conditions, with nozzle conditions in the range of  $NPR=2-9$ , throat area control injection pressure ratios of 0.9 to 2.4, and fluidic thrust vector control weight flow ratios (divergent duct injection/primary) up to 0.2.

Although a pitch thrust-vectoring efficiency of  $\eta=2.1^\circ/\% \text{-injection}$  and a yaw thrust-vectoring efficiency of  $\eta=1.2^\circ/\% \text{-injection}$  were achieved at  $NPR=4$ , both were with 2% injection. Thrust performance was exceptional at these conditions, with  $C_{fg,sys}=0.984$  and  $C_{fg,sys}=0.977$  achieved during pitch and yaw thrust-vectoring, respectively. A yaw thrust-vector angle of  $\delta_y=8.54^\circ$  was achieved at  $NPR=4$  with 5.8% injection and a thrust ratio of  $C_{fg,sys}=0.964$ . However, a pitch thrust-vector angle of  $\delta_p=6.4^\circ$  required 19.8% injection, while thrust ratio was  $C_{fg,sys}=0.951$ . The results from this test have not been formally published, but data is available upon request.

**Hybrid 2D CD:** The Hybrid 2D CD Nozzle geometry had a fixed exit, a hybrid (mechanical and fluidic) thrust vectoring capability, and ejectors. Experimental testing in JETF and a computational analysis were performed to understand the complex flow interactions between the ejector flow, the fluidic injection flow, and the primary exhaust nozzle flow. A side view sketch of the Hybrid 2D CD Nozzle design and a photograph of an oblique view of the model mounted in JETF are shown in figures 6(a) and 6(b), respectively. Three configurations were tested: a dry power hybrid thrust vectoring nozzle with  $NPR_D=20.6$ , a dry power fluidic thrust vectoring cruise nozzle with  $NPR_D=20.6$ , and an afterburning fluidic thrust vectoring nozzle with  $NPR_D=7.1$ . The geometric variables investigated include multi-slot injection with upper and lower divergent flap ejectors. The nozzle concept was tested at static freestream conditions, with nozzle conditions in the range of  $NPR=2-12$ , fluidic injection conditions in the range of  $SPR=0.6-1.5$ , and ejector pressure ratios less than twice the ambient pressure.

Results indicated that large pitch thrust-vector angles can be achieved with a combination of mechanical and fluidic thrust vectoring. The dry power hybrid thrust vectoring nozzle reached  $\delta_p=28^\circ$  at a  $NPR=5$  with 10.7% injection. Pitch thrust-vector

angles up to  $\delta_p=9^\circ$  were obtained at  $NPR \leq 5$  with 5.3% injection. The forward and aft injection slot combination provided larger pitch thrust-vector angles at lower NPR with the afterburning nozzle, and achieved larger pitch thrust-vector angles over the entire range of NPR with the dry power cruise nozzle, compared with single slot injection. The forward injection slot produced shock impingement (and reflection) on the opposite wall, which reduced nozzle performance, while the aft injection slot alleviated shock impingement problems at all SPR. The ejector provided critical performance benefits, but did not improve thrust-vector angle. Overall, the best thrust-vectoring efficiency achieved with the hybrid thrust vectoring configuration was  $\eta=2.6\%/\%-injection$  at a  $NPR=6$ , while the fluidic-only vectoring configuration achieved  $\eta=1.1\%/\%-injection$  at a  $NPR=10$ . Thrust performance for the hybrid configuration was not available, but the fluidic-only configuration with ejector flow reached thrust ratios of  $C_{fg,sys}=0.97$  for  $NPR > 5$ . A complete set of results is compiled in reference 7.

**AXI CD:** The primary goal of this test was to determine if comparable fluidic thrust vectoring performance could be achieved in an axisymmetric CD nozzle, as in 2D CD nozzles. A side view and an end view sketch of the AXI CD Nozzle are shown in figures 7(a) and 7(b), respectively. The geometric variables investigated were injection pattern (slot or holes), injection location (aft or forward), and number of injection slots (single or triple). The nozzle was tested at static freestream conditions, with nozzle conditions in the range of  $NPR=2-10$ , and with fluidic injection conditions up to  $SPR=1.5$ . The design nozzle pressure ratio was  $NPR_D=8.26$ .

Results indicated that an AXI CD nozzle can provide significantly better thrust efficiency, with slightly lower thrust-vector angles than a fluidic thrust vectored 2D CD nozzle at design conditions. The axisymmetric geometry improved thrust efficiency by providing pressure relief around the injection slot that is not available in 2D CD nozzles because the injection slot spans the width of the divergent flap. Thrust-vector angles of  $\delta_p=18^\circ$  at  $NPR=3$  and  $\delta_p=12.5^\circ$  at  $NPR_D=8.26$  were achieved with a secondary flow rate equal to 12% of the primary flow rate. This concept had a maximum thrust-vectoring efficiency of  $\eta=2\%/\%-injection$  ( $\delta_p=16^\circ$  with 8% fluidic injection) at  $NPR=2$ , but thrust ratio at this off-design condition was only  $C_{fg,sys}=0.895$ . At the design condition, thrust ratio improved to  $C_{fg,sys}=0.95$ , but thrust-vectoring efficiency was decreased to  $\eta=1.2\%/\%-injection$ .

Injection location (forward-, aft- or triple-slot) and injection pattern (slot or holes) had only minor effects on thrust vectoring. In general, the forward slot was slightly more effective at thrust vectoring the primary jet at overexpanded conditions with  $SPR < 0.08$  than the aft-slot, triple-slot or hole-injection pattern. The forward slot configuration had less flow separation on the injection-opposing wall than the other injection configurations. At  $SPR > 0.08$ , the primary jet flow that was diverted around the slot pressurized the injection-opposing wall, which reduced thrust-vector angle. A complete set of results is compiled in reference 8.

**Fluidic Jet Effects Model:** The goal of this research was to determine the freestream flow effects on fluidic thrust vectoring. The Fluidic Jet Effects Model (FJEM) was a 2D CD nozzle with a fluidic injection slot along the divergent wall for pitch thrust vectoring. Figure 8(a) shows a sketch of the model mounted to a sting-strut for experimental testing and figure 8(b) shows a representation of the instrumentation section and nozzle with the near sidewall removed. A bellows failure has delayed experimental testing of FJEM, but a new bellows design is underway. A computational effort has been completed using PAB3D with two-equation turbulence closure and linear Reynolds stress modeling. The nozzle was tested computationally with a static freestream  $M=0.05$  and with freestream Mach numbers of  $M=0.3-1.2$ . The range of nozzle conditions was  $NPR=3.6-7.2$  and fluidic injection conditions were set at either  $SPR=0.6$  or  $SPR=1.0$ . The design nozzle pressure ratio was  $NPR_D=14.6$ .

Computational results indicate that the external freestream flow decreases fluidic thrust vectoring effectiveness by  $1.5^\circ$  to  $2.9^\circ$  over the simulated range of NPR and Mach numbers. Compared with a static freestream, wind-on freestream flow decreased the pressure of the internally separated flow downstream of the injection slot and caused the shock to move further upstream on the wall opposite of the fluidic injection. The largest effects occurred at the most off-design conditions, when more separated flow existed in the nozzle. For example, thrust efficiency at wind-on freestream conditions was decreased 4.1% from the thrust performance at static freestream conditions with a  $NPR=3.6$ , compared to a 0.83% reduction from static freestream conditions at a  $NPR=7.2$ . As the shock moved further upstream at lower NPR, thrust efficiency was degraded by lack of flow expansion, reduced flow momentum at the nozzle exit, and increased total pressure losses. This concept achieved thrust-vectoring efficiencies from  $\eta=3.3\%/\%-injection$  at  $NPR=3.6$  to  $\eta=1.7\%/\%-injection$  at  $NPR=7.2$ . As with the previous SVC

concepts, the largest thrust ratio penalty occurred with the highest thrust-vectoring efficiency. A complete set of results is compiled in reference 9.

**Multi-Slot Injection:** The goal of this project was to enhance the thrust vectoring capability of a single slot injection scheme, without increasing the secondary flow requirements or incurring any performance penalties. The test nozzle was a 2D CD nozzle with a slot located on the divergent flap for fluidic pitch thrust vectoring. A side view sketch of the upper half of the Multi-Slot Injection Nozzle is shown in figure 9. The configurations tested included a baseline nozzle ( $NPR_D=8.78$ ) with a single injection slot and four dual injection slot configurations. The geometric variable under investigation was distance between the dual injection slots. All configurations had the same injection area to keep mass flow constant for a given pressure. The concept was tested at static freestream conditions, with nozzle conditions in the range of  $NPR=2-10$ , and injection conditions of  $SPR\leq 1.0$ . Computational modeling of two configurations using linear two-equation turbulence closure was completed with PAB3D at  $NPR\leq 10$  and  $SPR=0.7$ .

Results indicated that dual injection slots are beneficial at off-design conditions compared to the baseline, single slot injection configuration. Dual injection slots improved thrust vectoring and thrust efficiency ratio with high SPR at  $NPR<4$  compared to the baseline. However, there was no benefit to dual injection slots at  $NPR>4$ . Thrust vectoring efficiencies of  $\eta=2.4\%/\text{-injection}$  and  $\eta=1.2\%/\text{-injection}$  were achieved at  $NPR=3$  and  $NPR=7$ , respectively. System thrust ratios were not calculated for this concept because adequate secondary flow instrumentation was not available. Simulation of the slot and fluidic injection plenum geometry with computational grid was required to accurately predict nozzle performance. As found in other computational efforts like reference 9, a simple surface boundary condition for the injected flow was not sufficient for capturing all the physics and for predicting performance. A complete set of results is compiled in reference 10.

#### Throat Shifting Method

The hypothesis of the throat shifting method is that thrust vectoring occurs by shifting the throat of the nozzle with forced, asymmetric secondary fluidic injection. In a non-vectoring mode, the sonic plane or "throat" of the nozzle occurs at the nozzle's geometric minimum area. In a thrust-vectoring mode, the secondary air stream creates a new skewed aerodynamic minimum area, which shifts the location

of the throat from the geometric minimum area to the newly created aerodynamic minimum area. Flow turning then occurs in the subsonic flow region ahead of the new throat. Subsonic flow turning minimizes thrust losses. The resulting asymmetric pressure loading on the nozzle surfaces causes a thrust-vector angle of the primary exhaust flow.

In practice, an asymmetric pressure loading and primary flow thrust-vector angle can be created without completely shifting the throat location. For example, at some conditions, the throat did not technically shift in the Fluidic Yaw Vector Nozzle or in the Recessed Cavity Nozzle described below, but the sonic line was modified enough to create an asymmetric pressure loading and generate thrust vectoring from the asymmetric fluidic injection. Secondary injection mass-flow rate and pressure amplify asymmetric pressure loading.

**Fluidic Yaw Vector Nozzle:** The goal of this work was to determine internal performance of a convergent nozzle designed with a curved-bicuspid (lemon-shaped) cross section and a fixed aperture. The nozzle geometry was designed to complement the TS technique and to provide favorable airframe integration and structural characteristics. The geometric variables investigated include a single- and a twin-engine configuration with several injection patterns, injection locations and injection spans. In addition, an asymmetric aft deck was also tested to simulate nozzle integration with the aft fuselage of an airplane. A top view sketch of the single-engine configuration is shown in figure 10(a) and photograph of an end view of the twin-engine model, with lower aft deck, mounted in JETF is shown in figure 10(b). This concept was tested at static freestream conditions, with nozzle conditions in the range of  $NPR=1.4-4.0$ , and fluidic injection flow rates up to 15% of the primary flow rate. The design condition for a convergent nozzle is  $NPR_D=1.89$ .

Contrary to the hypothesis of the throat shifting method, results indicated that complete shifting of the throat was not required for thrust vectoring. At  $NPR=2$ , the throat shifted in alignment with the injection slot at all injection flow rates. However, at  $NPR=2.5-4$ , the throat completely shifted only for injection flow rates greater than 7% of the primary flow rate. For example, at  $NPR=2$ , the throat shifted 45° to align with the injection holes located at the 45° trailing edge of the twin-engine configuration, with as little as 2% injection, but thrust-vector angle increased only 3.3°. Increasing injection flow rate to 15% increased thrust-vector angle to 22° at  $NPR=2$ . The twin-engine configuration with a 45° injection hole pattern achieved  $\eta=1.8\%/\text{-injection}$  and  $C_{fg,sys}=0.948$  at  $NPR=3$ . Surface pressurization was a

function of injection flow rate, such that increased flow rate increased pressurization and improved thrust vectoring. Unfortunately, the single-engine configuration was unsuccessful at vectoring the primary jet thrust; the fluidic injection created counter-acting forces that resulted in a zero degree thrust-vector angle. The CFD code PAB3D was used to predict the nozzle performance of the twin-engine configuration and the results are documented in reference 11.

**Recessed Cavity Nozzle:** The goal of this NASA LaRC developed concept was to improve the thrust vectoring capability of the throat shifting method without compromising thrust efficiency. This nozzle was designed with a "recessed cavity", in which secondary air is injected asymmetrically upstream of the cavity to induce flow separation and cause pitch thrust vectoring of the primary exhaust jet. A side view sketch of the Recessed Cavity Nozzle concept is shown in figure 11. The investigative approach encompassed a parametric CFD investigation using PAB3D and an experimental validation of the concept at JETF. The geometric variables investigated include cavity divergence and convergence angle, cavity length and depth, injection angle, upstream minimum height, aft deck angle and aft deck curvature. Simulations were computed with a static freestream, with nozzle conditions set at  $NPR=3.9$ , and with a fluidic injection flow rate of 6% of the primary flow rate. Since the geometry is not convergent or convergent-divergent in nature, it is more difficult to quote a design nozzle pressure ratio for this concept. However, data indicated a  $NPR_p \approx 3$  based on experimental thrust ratio without fluidic injection.

Results for the symmetric nozzle (no aft deck) indicated that fluidic injection can control flow separation in the recessed cavity and enhance the TS thrust vectoring capability. Large thrust-vector angles were achieved with minimal impact on thrust efficiency ( $\delta_p = 14.67^\circ$ ,  $\eta = 2.15\%/\text{injection}$ , and  $C_{fg,sys} = 0.957$ ). The separated flow in the recessed cavity caused much lower pressure ratios ( $p/p_{t,j} \approx 0.2$ ) along the wall than would be expected from the Mach number present in the cavity and compared to previously tested nozzles using the TS method ( $p/p_{t,j} = 0.5-0.6$ ). The cavity allowed the wall pressure to be pumped down by the primary flow, which improved thrust-vector angle compared to throat shifting concepts without a recessed cavity.

Thrust vectoring was achieved without completely shifting or skewing the throat at some conditions. Increasing injection angle (more upstream) or cavity convergence angle improved thrust-vectoring efficiency, with only a minimal

impact on thrust ratio. Decreasing upstream minimum height improved thrust-vector angle, but resulted in a 2.2% penalty in thrust ratio. Decreasing cavity length improved thrust ratio by 1.6% and increased thrust-vector angle slightly.

A nozzle aft deck is used for shielding purposes and was studied in this investigation to understand the impacts of aircraft integration on fluidic thrust vectoring. The thrust vectoring capability of the concept with the inclusion of an aft deck was dependent on aft deck angle (figure 12(a)) and curvature (figure 12(b)). A  $0^\circ$  straight aft deck was detrimental to the thrust vectoring capability, but a  $20^\circ$  straight aft deck achieved thrust-vectoring efficiencies of  $\eta = 1.7-3\%/\text{injection}$ . One of the curved aft decks eliminated the inherent thrust-vector angle (at  $NPR=3.9$ ) that resulted from having an asymmetric geometry. The rotated tangent arc deck configuration had a  $\delta_p = 0.3^\circ$  thrust-vector angle in the non-vectoring mode and a range of thrust-vector angles in the vectored mode from  $\delta_p = -8^\circ$  to  $\delta_p = 11^\circ$ . Computational results are published in reference 12.

#### Combined Shock Vector Control and Throat Shifting Methods

This technique combines the shock vector control and throat shifting methods described above, for multi-axis thrust vectoring.

**MATV Legacy Yaw Vector:** The goal of this activity was to expand the capability of a stellar fluidic yaw-thrust vectoring nozzle to include a multi-axis thrust vectoring capability. Although the nozzle used the combined techniques of throat shifting in the yaw axis and shock vector control in the pitch axis, the design was originally optimized for the TS technique. Seventeen configurations were tested with geometric variables including three injection schemes for pitch thrust vectoring, with four injection locations per scheme and four aft deck configurations. The nozzle was tested at static freestream conditions, with nozzle conditions in the range of  $NPR=3-10$ , and fluidic injection rates up to 10% of the primary flow rate.

Retrofitting the existing nozzle optimized and designed for yaw thrust vectoring with the throat-shifting method did not provide significant pitch thrust-vector angles. At an  $NPR=5$ , a range of pitch thrust-vector angles from  $\delta_p = -3^\circ$  to  $\delta_p = 4^\circ$  was achieved. The aft deck adversely affected pitch thrust vectoring performance. Results of this test have not been formally published.

### Counterflow Method

The hypothesis of the counterflow method is that thrust vectoring occurs by creating counterflowing primary and secondary air streams with the application of suction at a slot between the primary nozzle and an aft collar, as shown in figure 13(a) (ref. 24). However, research has revealed that at some flow conditions and geometric configurations, coflowing primary and secondary streams also produces thrust vectoring. A vacuum is applied to a plenum that feeds a suction slot between the exit of the primary exhaust nozzle and a shrouded collar. Mixing occurs in the shear layers between the primary flow and the suction flow, but the presence of the collar prohibits mass entrainment. The flow accelerates near the collar and the pressures drop. The asymmetric pressure loading on the collar surfaces then creates thrust vectoring.

Counterflow-I: The goal of the first counterflow concept was to determine thrust vectoring and nozzle performance over a wide range of operating conditions on a larger-scale nozzle ( $A_t=3 \text{ in}^2$ ) than the first laboratory tests ( $A_t=0.62 \text{ in}^2$ ). A side view sketch of the Counterflow Nozzle concept is shown in figure 13(a). The photograph of the model with the near sidewall removed is shown in figure 13(b). The geometric variables investigated include suction slot height and collar geometry. The nozzle was tested at static freestream conditions, with nozzle conditions in the range of  $\text{NPR}=3.5\text{-}10$  and secondary suction pressures in the range of  $\Delta p_{\text{slot}}=0.5\text{-}7.8 \text{ psi}$ . The design condition of the primary nozzle was  $\text{NPR}_D=7.82$ .

The potential drawback of the counterflow method was found to be jet attachment of the primary jet to the suction collar that occurs at certain conditions and various geometric configurations. The problem is hysteretic in nature and not easily controllable. However, the counterflow method has huge promise if jet attachment could be completely avoided through proper nozzle design. For example, at  $\text{NPR}=8$  and jet unattached conditions, thrust-vector angle was  $\delta_p=12^\circ$  and thrust ratio was  $F/F_i=0.945$  with a secondary weight flow rate less than 1% of the primary weight flow rate. A maximum thrust-vector angle of  $\delta_p=15^\circ$  was achieved at  $\text{NPR}=5$ , but with a higher thrust penalty ( $F/F_i=0.92$ ). Increasing ejector pressure, slot height and collar length resulted in larger thrust-vector angles. However, increasing ejector pressure and collar length also increased the risk of jet attachment. Decreasing slot height caused jet attachment at some conditions, but also improved thrust efficiency of jet unattached cases. Beyond causing thrust vectoring, applied suction increases

mixing between the secondary and primary flows, which shortens the length of the plume and potentially improves nozzle cooling. Critical design work would be required to obtain the best geometry for optimum performance. Experimental results are compiled in reference 13.

Counterflow-II: The goal of the second counterflow test entry was to analyze methods for alleviating jet attachment. The geometric variables investigated include various porous collar inserts, slot height and a modified collar shape and surface roughness. Results indicate that a porous collar geometry does not prevent jet attachment as hypothesized. Truncating the collar did reduce the likelihood of jet attachment, but a reduction in slot height increased the probability of jet attachment. At jet unattached conditions, reducing slot height increased resultant thrust ratio at the expense of decreased pitch thrust-vector angle. Results from this experiment have not been formally documented.

Counterflow CFD: The primary goal of the computational assessment of the counterflow thrust vectoring method was to understand the physics of the counterflowing and coflowing shear layers that develop at different conditions. A secondary goal was to achieve the first successful CFD simulations of the counterflow thrust vectoring concept. Two-dimensional, structured-grid simulations were computed using PAB3D with 2-equation turbulence closure and a linear Reynolds stress model. The primary nozzle had an expansion ratio of 1.69 for a design condition of  $\text{NPR}_D=7.82$ . An 8" long curved suction collar geometry was selected for the computational study. The method was simulated with primary flow conditions of  $\text{NPR}=8$  and suction slot pressures ranging from 1 to 6 psi below ambient. A suction parameter ( $\lambda$ ), defined in the nomenclature section, was an independent input variable used for plotting experimental and computational data.

The computational assessment revealed significant differences in jet attachment between 2D simulations and the 2D experiment. Computations indicated that jet attachment occurred at  $\lambda > 0.4$ , whereas experimental jet attachment occurred at  $\lambda > 0.22$  for the same configuration. This indicates an unfortunate result that the hysteretic jet attachment is condition- and geometry-dependent, and difficult to control.

There was an excellent correlation of thrust-vector angle between experiment and computation up to  $\lambda = 0.22$ , prior to experimental jet attachment. Predicted nozzle discharge coefficient correlated within 0.2% of experimental data. As expected from

2D simulations that do not include the viscous effects on the sidewalls that are present in the experiment, nozzle thrust efficiency was predicted 0.5-0.7% higher than experimental data at jet unattached conditions. Both experiment and computations indicate only a 1.5% penalty in thrust ratio for using the counterflow thrust vectoring method. Computational details revealed that thrust vectoring occurred and that a countercurrent shear layer developed in both the coflowing and counterflowing streams. Therefore, thrust vectoring is not dependent on counterflowing primary and secondary streams and may simply result from asymmetric separation control that is modified through applied suction. Detailed computational results are compiled in reference 14.

#### Comparison of Fluidic Thrust Vectoring Methods

Representative system thrust performance and thrust-vectoring efficiencies of the shock vector control and the throat shifting concepts investigated at NASA LaRC are compiled in figures 14 and 15, respectively. The reader is encouraged to look to specific references for more data, since these charts only include a sampling of the data. Additionally, the figures include  $NPR_D$  in the legend for each configuration because of the difficulty in comparing the assortment of concepts with various design points.

Expectations are that throat shifting concepts (subsonic flow turning) offer higher thrust efficiency than concepts implementing the shock vector control method (supersonic flow turning), while SVC concepts usually provide larger thrust-vector angles. However, in order to achieve large thrust-vector angles, SVC concepts must operate at off-design, highly over-expanded conditions. Therefore, SVC concepts are plagued not only with thrust losses from flow turning through the shock, but also from over-expansion losses.

Although more SVC concepts have been tested at NASA LaRC than TS concepts, in general, data supports expectations, with throat shifting concepts providing higher thrust efficiencies (for  $NPR < 5$ ) than SVC concepts (figure 14). Nozzle concepts using the shock vector control method generally produced thrust ratios ranging from  $C_{fg,sys}=0.86$  to  $C_{fg,sys}=0.94$ , with one ejector-aided SVC concepts reaching  $C_{fg,sys}=0.97$ . Thrust ratios for nozzles using the throat shifting method tended to range from  $C_{fg,sys}=0.94$  to  $C_{fg,sys}=0.98$  (see figure 14 and referenced data).

In addition, several of the SVC concepts provided better thrust-vectoring efficiencies than the TS concepts ( $NPR < 5$ ), as expected (figure 15). Thrust-vectoring efficiencies up to  $\eta=4^\circ/\%-injection$

were achieved with shock vector control concepts, but generally ranged from  $\eta=0.9^\circ/\%-injection$  to  $\eta=2.8^\circ/\%-injection$ . Thrust-vectoring efficiencies for concepts using the throat shifting method ranged from  $\eta=1.4^\circ/\%-injection$  to  $\eta=2.2^\circ/\%-injection$ . However, current research programs are focused on techniques to improve the thrust-vectoring efficiency of the throat shifting method without compromising thrust efficiency (refs. 12, 27, 28).

The counterflow method was not included in figures 14 and 15 because there is no straightforward way to compare secondary suction to the fluidic injection techniques. The range of thrust ratios achieved with the counterflow method was from  $C_{fg,sys}=0.92$  to  $C_{fg,sys}=0.97$ . The counterflow method is an appealing thrust vectoring method, but issues such as suction supply source, hysteresis effects, and airframe integration need to be addressed.

#### CONCLUSIONS

In general, results from the fluidic thrust vectoring research conducted at NASA Langley Research Center indicated that the throat shifting method was most thrust efficient of the fluidic thrust vectoring methods, but larger thrust-vector angles were obtained with the shock vector control method. However, promising new approaches to the throat shifting method are improving thrust-vector angles without comprising thrust efficiency. The counterflow method is an appealing thrust vectoring method, but issues such as suction supply source, hysteresis effects, and airframe integration need to be addressed. Some specific results from the fluidic thrust vectoring tests conducted at NASA LaRC include:

1. Contrary to original hypothesis, complete shifting of the aerodynamic throat was not required for thrust vectoring with the throat shifting method of fluidic thrust vectoring. Likewise, counterflowing primary exhaust jet and secondary suction streams were not required for thrust vectoring with the counterflow method of fluidic thrust vectoring.
2. Shock vector control concepts obtained thrust-vectoring efficiencies between  $0.9^\circ/\%-injection$  and  $4^\circ/\%-injection$  with system thrust efficiencies in the range of 0.86 to 0.94. Avoiding shock impingement on the opposite nozzle wall was critical for reaching high thrust efficiency and large vector angles with the shock vector control method.
3. Throat shifting concepts achieved thrust-vectoring efficiencies between  $1.4^\circ/\%-injection$

- and 2.2%/-injection, with system thrust efficiencies in the range of 0.94 to 0.98.
4. The Recessed Cavity Nozzle, a recently enhanced throat shifting concept, vectored the primary jet 3%/-injection in the negative direction and 1.76%/-injection in the positive direction with an aft deck.
  5. The Hybrid 2DCD and the Multi-Slot Injection Nozzle indicated a benefit of dual-injection slots over single-injection slots, but only for limited nozzle pressure ratios and secondary to primary total pressure ratios.
  6. Results from several tests; the Fluidic Yaw Vector Nozzle, the legacy Multi-Axis Thrust Vectoring Nozzle, and the Recessed Cavity Nozzle, indicated the difficulty of thrust vectoring with the inclusion of an aft deck. However, significant ranges of thrust-vector angle were achieved with several Recessed Cavity Nozzle, aft deck configurations. In addition, the inherent thrust-vector angle caused by the asymmetric deck geometry was eliminated with some aft deck curvature.
  7. Injection angle was a geometric variable that proved to be critical for achieving large thrust-vector angles. The Recessed Cavity Nozzle showed an improvement of 4° in thrust-vector angle by simply directing the fluidic injection flow upstream toward the oncoming, primary exhaust flow at an injection angle of 150°, compared to injecting normal to the flow.

#### REFERENCES

1. Walker, S. H.: *Lessons Learned in the Development of a National Cooperative Program*. AIAA 97-3348. 1997.
2. Abeyounis, W. K.; and Bennett, B. D. Jr.: *Static Internal Performance of an Overexpanded, Fixed-Geometry, Nonaxisymmetric Nozzle With Fluidic Pitch-Thrust-Vectoring Capability*. NASA TP-3645, October 1997.
3. Wing, David J.: *Static Investigation of Two Fluidic Thrust-Vectoring Concepts on a Two-Dimensional Convergent-Divergent Nozzle*. NASA TM-4574, December 1994.
4. Chiarelli, C.; Johnsen, R. K.; Shieh, C. F.; Wing, D. J.: *Fluidic Scale Model Multi-Plane Thrust Vector Control Test Results*. AIAA 93-2433, June 1993.
5. Giuliano, V. J.; and Wing, David J.: *Static Investigation of a Fixed-Aperture Exhaust Nozzle Employing Fluidic Injection for Multiaxis Thrust Vector Control*. AIAA 97-3149, July 1997.
6. Federspiel, J. F.; Bangert, L. S.; Wing, D. J.; and Hawkes, T.: *Fluidic Control of Nozzle Flow - Some Performance Measurements*. AIAA 95-2605, July 1995.
7. Anderson, C. J.; Giuliano, V. J.; and Wing, David J.: *Investigation of Hybrid Fluidic / Mechanical Thrust Vectoring for Fixed-Exit Exhaust Nozzles*. AIAA 97-3148, July 1997.
8. Wing, David J.; and Giuliano, V. J.: *Fluidic Thrust Vectoring of an Axisymmetric Exhaust Nozzle at Static Conditions*. ASME FEDSM97-3228, June 1997.
9. Deere, K. A.: *Computational Investigation of the Aerodynamic Effects on Fluidic Thrust Vectoring*. AIAA 2000-3598, July 2000.
10. Waithe, K. A.: *An Experimental and Computational Investigation of Multiple Injection Ports in a Convergent-Divergent Nozzle for Fluidic Thrust Vectoring*. GWU Master's Thesis, May 2001.
11. Deere, K. A.: *PAB3D Simulations of a Nozzle with Fluidic Injection for Yaw Thrust-Vector Control*. AIAA 98-3254, July 1998.
12. Deere, K. A.; Berrier, B. L.; Flamm, J. D.; and Johnson, S. K.: *Computational Study of Fluidic Thrust Vectoring using Separation Control in a Nozzle*. AIAA 2003-3803, June 2003.
13. Flamm, J. D.: *Experimental Study of a Nozzle Using Fluidic Counterflow for Thrust Vectoring*. AIAA 98-3255, July 1998.
14. Hunter, C. A. and Deere, K. A.: *Computational Investigation of Fluidic Counterflow Thrust Vectoring*. AIAA 99-2669, June 1999.
15. A User's Guide to the Langley 16-Foot Transonic Tunnel Complex, Revision 1. NASA TM-102750, September 1990. (Supersedes NASA TM-83186.)
16. Berrier, B. L.; Leavitt, L. D.; and Bangert, L. S.: *Operating Characteristics of the Multiple Critical Venturi System and Secondary Calibration Nozzles Used for Weight-Flow Measurements in the Langley 16-Foot Transonic Tunnel*. NASA TM 86405, September 1985.
17. Abdol-Hamid, K. S.; Lakshmanan, B.; and Carlson, J. R.: *Application of Navier-Stokes Code PAB3D With k-ε Turbulence Model to Attached and Separated Flows*. NASA TP-3480, January 1995.
18. Balakrishnan, L.; and Abdol-Hamid, K. S.: *A Comparative Study of Two Codes with an Improved Two-Equation Turbulence Model For Predicting Jet Plumes*. AIAA 92-2604, June 1992.
19. Pao, S. P.; and Abdol-Hamid, K. S.: *Numerical Simulation of Jet Aerodynamics Using the Three-Dimensional Navier-Stokes Code PAB3D*. NASA TP 3596, September 1996.

20. van Leer, B.: *Flux-Vector Splitting for the Euler Equations*. ICASE Report 82-30, 1982.
21. Roe, P. L.: *Characteristics Based Schemes for the Euler Equations*. A Numerical Review of Fluid Mechanics, 1986, pp. 337-365
22. Abdol-Hamid, K. S.: *Implementation of Algebraic Stress Models in a General 3-D Navier-Stokes Method (PAB3D)*. NASA CR-4702, 1995.
23. Abdol-Hamid, K. S.: *Application of a Multiblock/ Multizone Code (PAB3D) for the Three-Dimensional Navier-Stokes Equations*. AIAA-91-2155, June 1991.
24. Panitz, T., and Wasan, D. T.: Flow Attachment to Solid Surfaces: The Coanda Effect. Al Ch E Journal, Volume 18, No. 1, January 1972.
25. Strykowski, P. J.; and Krothapalli, A.: *The Countercurrent Mixing Layer: Strategies for Shear-Layer Control*. AIAA 93-3260, July 1993.
26. Giuliano, V. J.; Flugstad, T. H.; Semmes, R.; and Wing, David J.: *Static Investigation and Computational Fluid Dynamics (CFD) Analysis of Flowpath Cross-Section and Trailing-Edge Shape Variations in Two Multiaxis Thrust Vectoring Nozzle Concepts*. AIAA 94-3367, June 1994.
27. Miller, D. N., Yagle, P. J., Hamstra, J. W.: *Fluidic Throat Skewing for Thrust Vectoring in Fixed Geometry Nozzles*. AIAA 99-0365, January 1999.
28. Yagle, P. J., Miller, D. N., Ginn, K. B., Hamstra, J. W.: *Demonstration of Fluidic Throat Skewing for Thrust Vectoring in Structurally Fixed Nozzles*. 2000-GT-0013, May 2000.

Test	Partners	Reference
2D CD PTV	LaRC, Rockwell	2
2D CD MATV	LaRC, Rohr	3, 4
Spherical Convergent Flap	LaRC, Pratt & Whitney	5
LOLA-II	LaRC, General Electric Aircraft Engines	6
Hybrid 2D CD	LaRC, Boeing Pratt & Whitney,	7
AXI-CD	LaRC, Pratt & Whitney	8
Jet Effects Model	LaRC	9
Multi-Slot Injection	LaRC, Pratt & Whitney	10

Table 1. Nozzle concepts using the shock vector control method for fluidic thrust vectoring.

Test	Partners	Reference
FYVN	LaRC, Pratt & Whitney	11
Recessed Cavity	LaRC	12

Table 2. Nozzle concepts using the throat shifting method for fluidic thrust vectoring.

Test	Partners	Reference
MATV	LaRC	None

Table 3. Nozzle concept using combined shock vector control and throat shifting methods for multiaxis fluidic thrust vectoring.

Test	Partners	Reference
Test-I, II	LaRC, Florida State University, University of Minnesota	13
CFD	LaRC	14

Table 4. Nozzle concepts using the counterflow method for fluidic thrust vectoring.

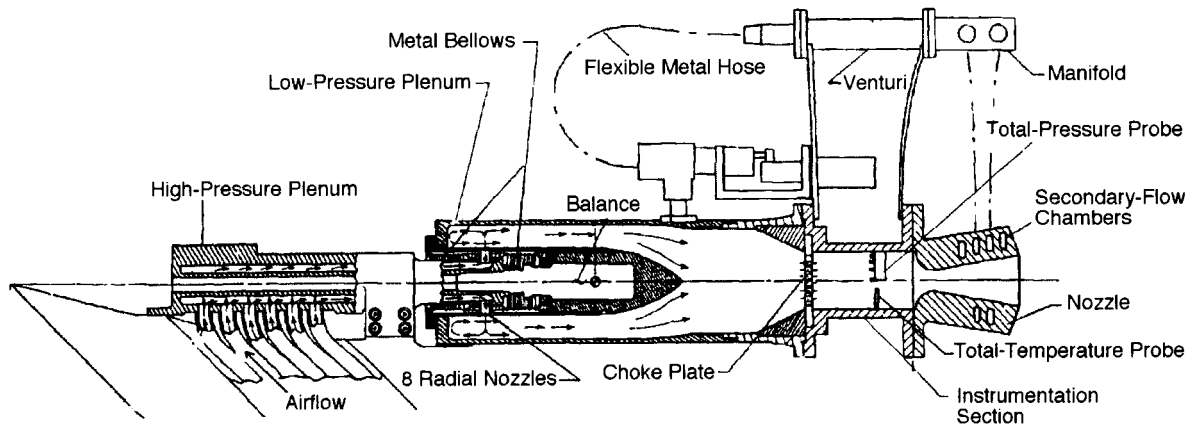
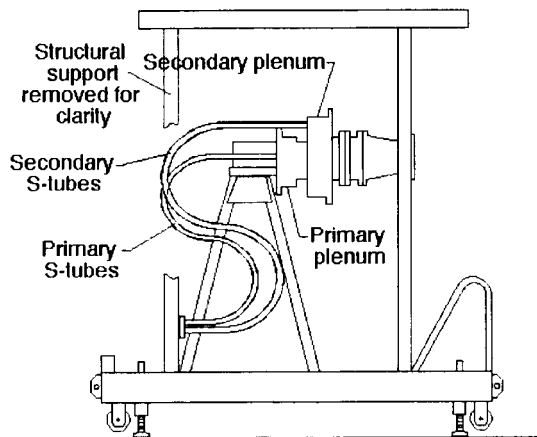
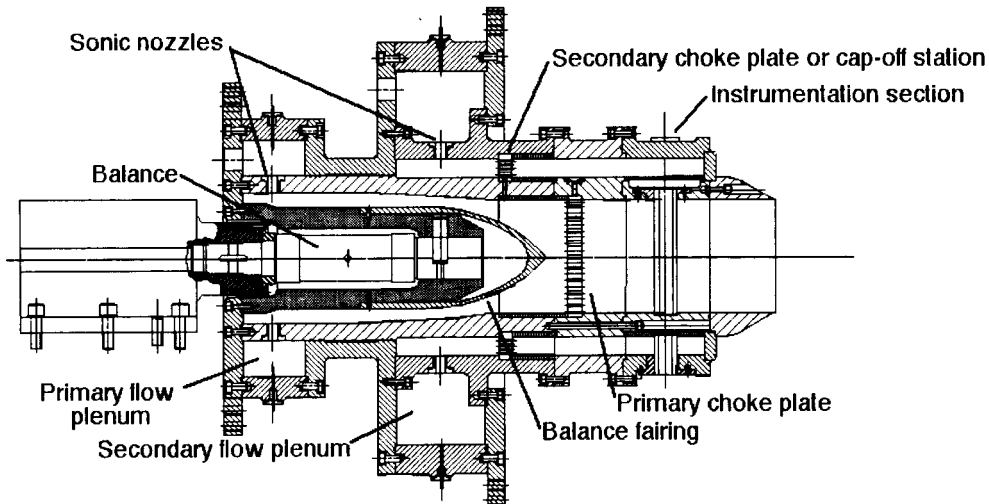


Figure 1. A side view of the 2D CD PTV Nozzle mounted on the single-engine propulsion simulation system.

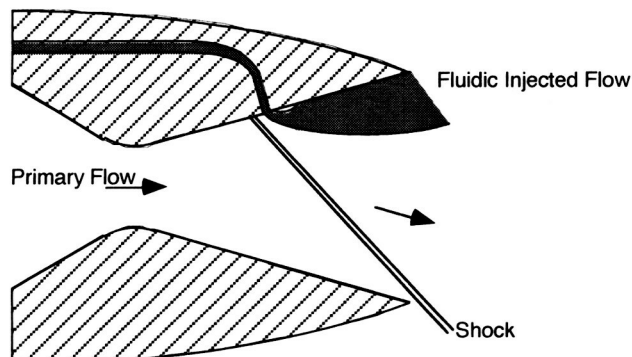


(a) Dual-flow propulsion simulation system mounted on the static thrust stand.

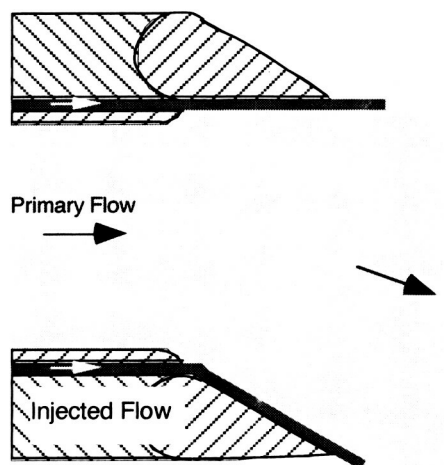


(b) Detail sketch of dual-flow hardware.

Figure 2. Dual-flow propulsion simulations system.

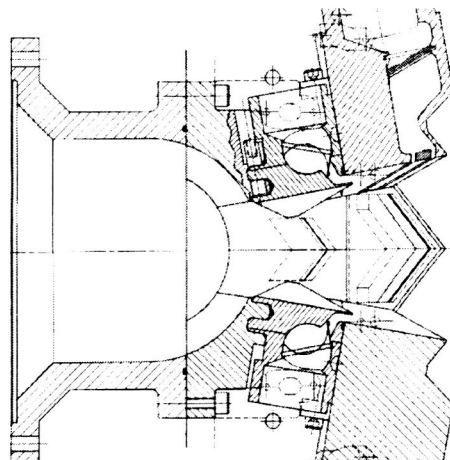


(a) Side view.

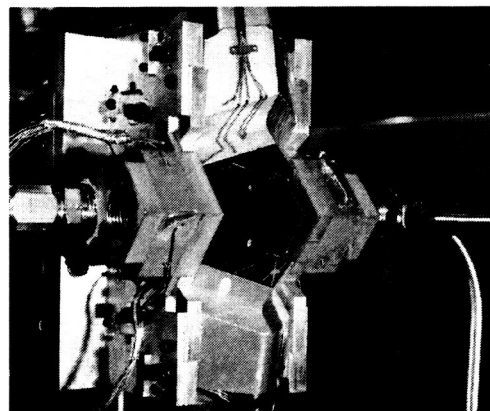


(b) Top view.

Figure 3. 2D CD MATV Nozzle.



(a) Side view.



(b) Oblique view of model mounted in JETF.

Figure 4. Spherical Convergent Flap Nozzle.

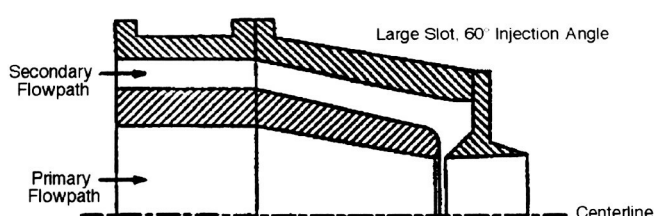
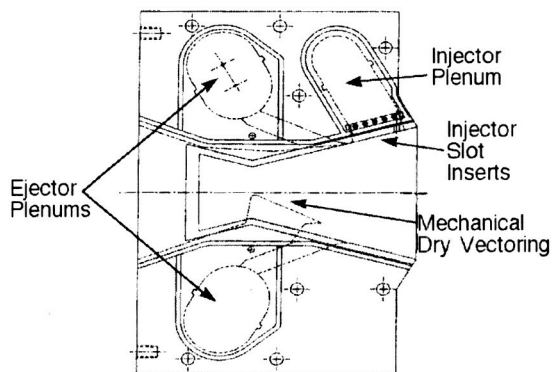
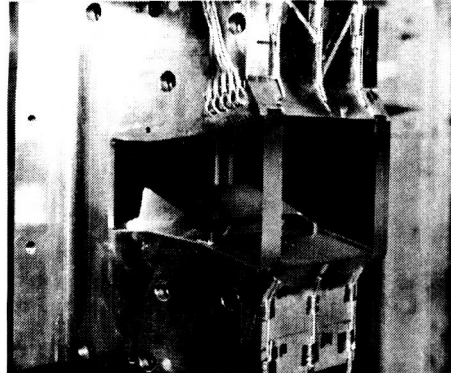
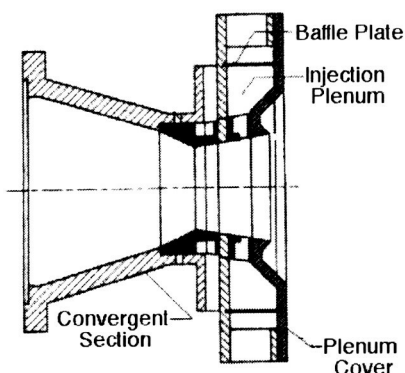


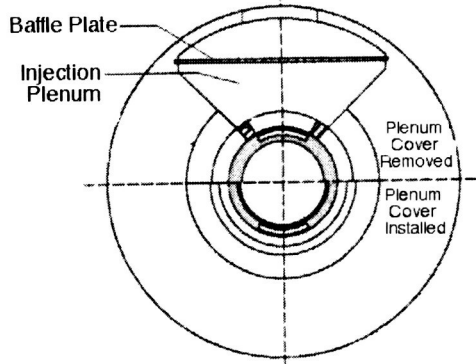
Figure 5. LOLA-I Nozzle.



(a) Side view.

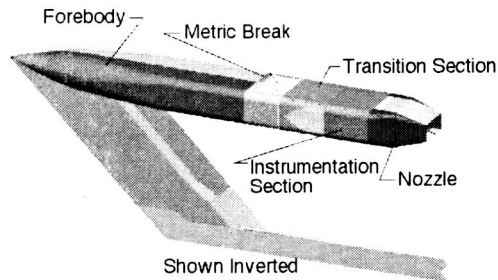
(b) Oblique view of model mounted in JETF.  
Figure 6. Hybrid 2D CD Nozzle.

(a) Side view.

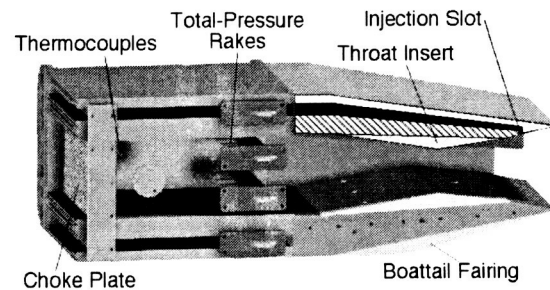


(b) End View.

Figure 7. AXI CD Nozzle.



(a) Model mounted to a forebody, sting, and strut.



(b) Instrumentation section and nozzle with near sidewall removed.

Figure 8. Fluidic Jet Effects Model.

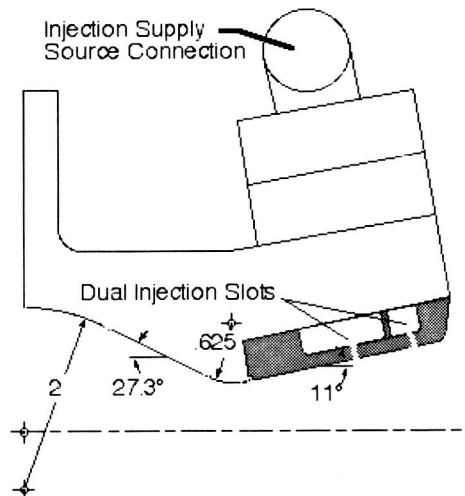
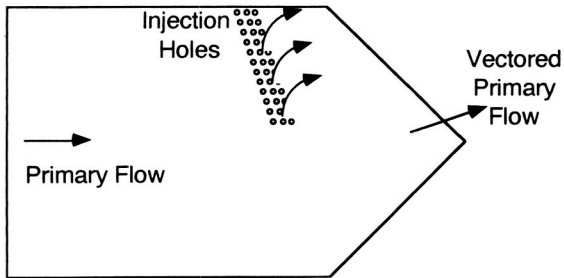
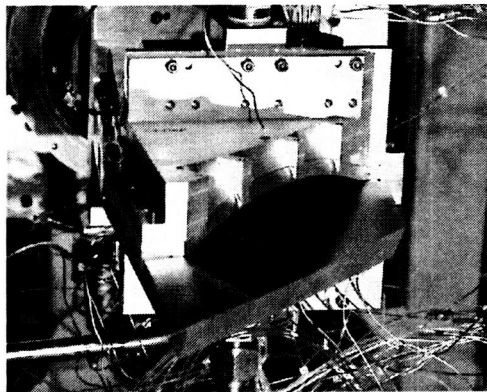


Figure 9. Side view of the upper half of the Multi-Slot Injection Nozzle.



(a) Top view of single-engine configuration.



(b) End view of twin-engine model with lower aft deck.

Figure 10. Fluidic Yaw Thrust Vectoring Nozzle.

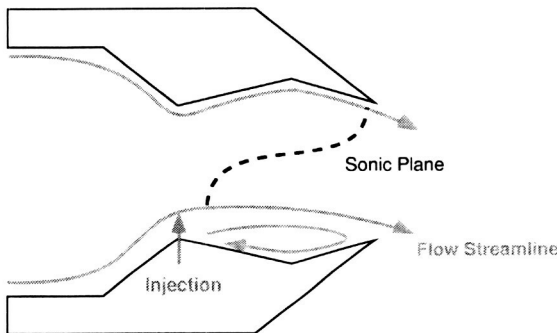
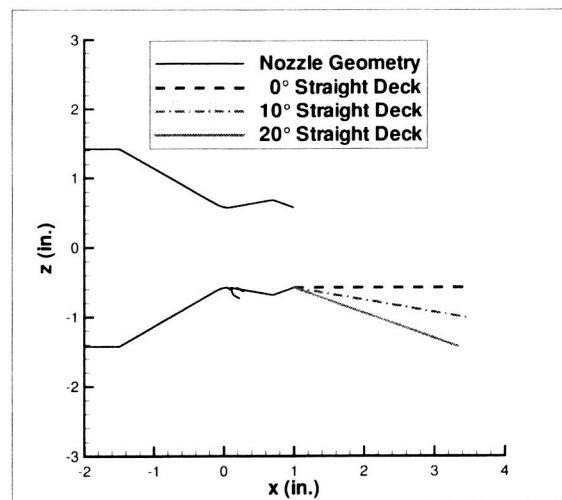
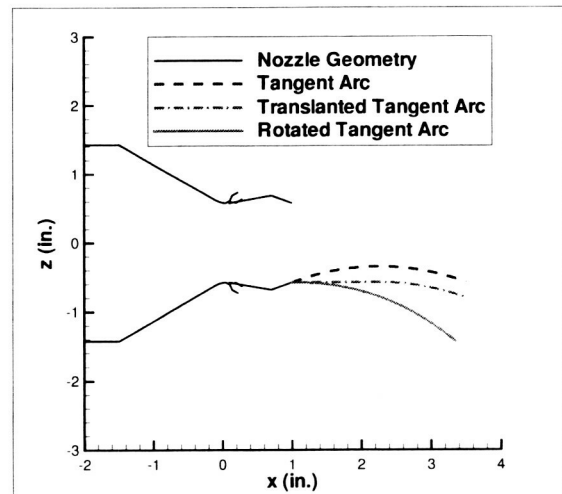


Figure 11. Side view of Recessed Cavity Nozzle



(a) Straight aft deck configurations.



(b) Curved aft deck configurations.

Figure 12. Recessed Cavity Nozzle, aft deck geometric configurations.

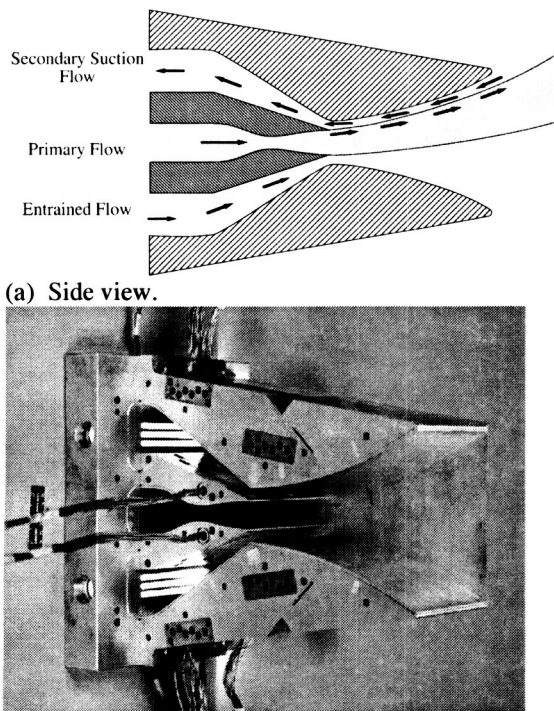


Figure 13. Counterflow Nozzle.

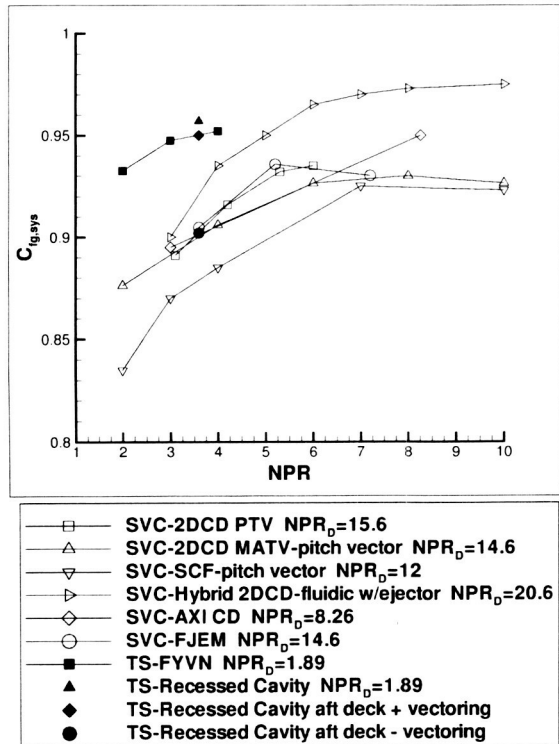


Figure 14. System thrust ratio data for configurations implementing the shock vector control (SVC) and throat shifting (TS) methods.

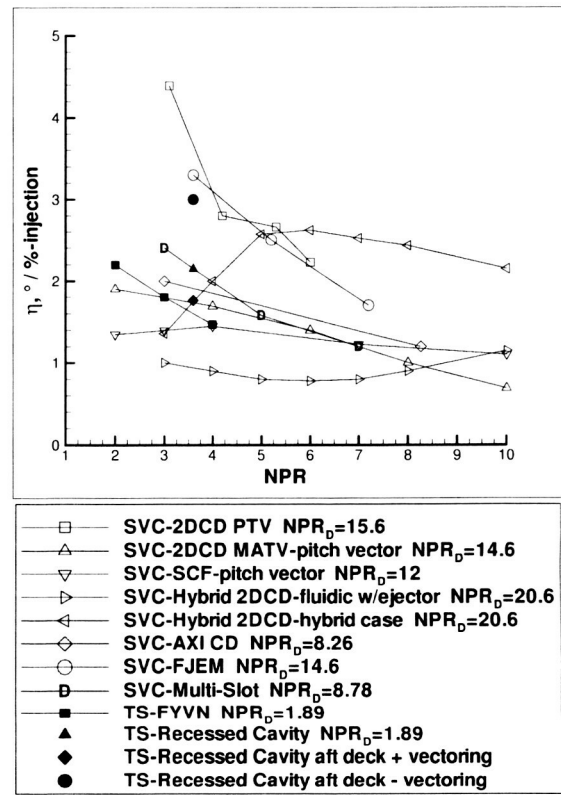


Figure 15. Thrust-vectoring efficiency data for configurations implementing the shock vector control (SVC) and throat shifting (TS) methods.